Desalination and Water Treatment
www.deswater.com

doi: 10.5004/dwt.2020.26076

198 (2020) 140–150
September

Seawater desalination by separating micro and nano salt particles with the use of magnetic and electric fields

Mohammad Vahedi Nejad, Hamid Reza Nazif*

Department of Mechanical Engineering, Imam Khomeini International University, Ghazvin, Iran, email: h_nazif@yahoo.com/nazif@eng.ikiu.ac.ir (H.R. Nazif)

Received 22 July 2019; Accepted 6 May 2020

ABSTRACT

In this research, a seawater electric-magnetic desalination system was studied and simulated. For the separation of salt particles with nano and micro sizes, the intensity of the electric and magnetic field and the seawater velocity play a dominant role in the separation system. The results for different variables such as magnetic and electric field, different diameters of particles, the inlet aspect ratio of the separator, and fluid flow rates were reviewed. It was observed that the separation efficiency of the electric-magnetic method decreased abruptly by 5% for the particles smaller than 100 nm. In addition, by increasing the aspect ratio, the percentage of particle discharge from the clean water zone decreased and the number of particles adsorbing to the electric and magnetic walls increased. Moreover, with increasing fluid velocity, the amount of particulate adsorption in the vicinity of the magnetic walls was significantly reduced. In this study, for a unit with dimensions of 60 cm × 10 cm × 20 cm and the particle input mass of 0.1 kg/s with a mean efficiency of 60% in voltage of 1 V and the magnetic field of 0.2 Tesla, the sweet water particles rate reduces to 0.006 kg/s.

Keyword: Multiphase flow; CFD; Desalination; Particle separation; Electric-magnetic force

1. Introduction

During the past century, abstracting freshwater from saltwater has attracted considerable attention. However, limits to freshwater availability in regions has suggested the need to use desalination technologies for the availability of affordable water. Typically, freshwater salinity is less than 1,000 ppm which is regarded as harmless drinking water and is useful for domestic and agricultural purposes [1]. Seawater salinity is approximately 35,000 ppm, salt salinity of the lake ranges from 50,000–270,000 ppm, and the average salinity of the Caspian Sea is about 12,000 ppm. The energy consumption of water desalination depends on the salt content. Saltwater appears desirable for use as human consumption and as irrigation with the aim of desalinating fresh water. Salt production is considered the consequence of the desalination process. Much new evidence on desalination investment has focused on affordable water resources development for human consumption. In addition to water from precipitation and wastewater recycling, desalination is considered as an alternative water supply source. Energy consumption and salinity level of desalination are two key factors in the desalination process. Thus, adopting a desalination method that has a lower energy requirement is an important factor in water desalination.

For separation of particles, scattering particles in fluid should be considered. Accordingly, Morsi and Alexander [2] studied the response of the motion of a spherical particle in a one-dimensional flow and the motion of a particle around a circular cylinder and an airfoil. Mohammadi and Kaviani [3] developed a method for sewage treatment

* Corresponding author.

by designing and constructing a very small empirical electrode electric cell and used the method to study the effects of different operating conditions such as flow velocity, voltage, and concentration on seawater behavior by electrodialysis. The flow of biomagnetic fluids in a channel under the influence of a magnetic field was studied by leukopalos and tetrazolacice [4]. The results of the field of velocity and temperature, shell stress, and heat transfer rate indicated that the presence of the magnetic field has a significant effect on the flow field. With the aid of particle adsorption, Mohammadi et al. [5] used Taguchi analytical method for the separation of copper ions. The use of electrodialysis in their study was to evaluate optimal laboratory conditions to achieve the highest removal percentage. In another study, anionic and cationic selector membranes were used. A two-dimensional magnetic system of suspended particles in silicon oil as a platform for biomass analysis was presented by Lehman et al. [6]. Paramagnetic microprocessors inside the droplets made the movement under the magnetic field. Furlani et al. [7] presented a model to predict the absorption of micro-magnetic nanoparticles in a microscopic system. This model was used to examine the distribution of particle size parameters including the size, material properties, applied flow, microchannel dimensions, fluid properties, and flow velocity. Nichols [8] studied fluid in a channel with a barrier in the presence of nanoparticles and magnetic fields. The purpose was that the cations and anions become isolated. They showed that the separation area decreases with an increasing magnetic field. Their studies indicate that increasing the strength of the magnetic field causes the axial velocity to be denser particles. Also, the shape of flow patterns started to change with the magnetic parameter changes. Alnaimat et al. [9] used a model for electromagnetic-mechanical desalination by simulating the operational parameters numerically. They modeled the fluid flow and the motion of charged particles based on the hydrodynamic forces of the electric field. They showed that a low velocity of fluid increases the residence time and separation efficiency of particles. They also showed that a combination of electric and magnetic forces can be effectively used for separating seawater from the saline solution. Zarzo and Prats [10] mainly investigated desalination performance and energy consumption, and various technologies available. Their research focused on reverse osmosis, which has numerous applications in technology. Rozanska et al. [11] studied ions removal by simple electrodialysis membranes and selectors. From their studies, it was found that increasing the fluid density cause a gradual increase of bivalent ions passing through the selective membrane, which does not correspond to the primary goal with the use of this membrane. In this case, the current density should be considered less than the limiting current density, thus, resulting in energy savings from the use of selector membranes. To reach resistance and to decide operating current, the limiting flow density plays an important part. In addition, the properties of the membrane and electrolyte solution, the flow velocity, and temperature and electrolysis structure are also other important parameters. The presence of different particles with different sizes is an inseparable part of saline water. In desalination, the particles having a diameter of around 0.5 nm to several microns are common [12]. Thus, a wide range of particles in the range of 0.1 nm to 100 μm are used in different studies. The effect of electrical and magnetic waves on the amount of water-soluble salt is investigated.

In this study, the laminar flow of water contains salt particles that are modeled by the Euler–Lagrangian method and solved using the finite volume method. The effect of changes to electric and magnetic fields on the separation rate of water-soluble particles in different diameters has been investigated. The results indicate that electric and magnetic field variations play an important role in the separation of ions. Also, separation system variations resulting from different inlet geometries can play a key role in increasing the separation percentage.

2. Governing equations

In the present study, Euler–Lagrangian method is used to simulate the laminar flow contains soluble salt particles for low Reynolds number (Re < 50). For free flow as the continuous phase, the steady-state solution is obtained using the Navier–Stokes equations. Also, a dynamic model is assumed for soluble salt particles as the discontinuous phase using the momentum equation (Newton's law). Here, the desalination process consists of the coupling of two methods. Regarding this, the effect of particles on the continuous phase was considered as the source term and the forces on the particles in the continuous phase are defined with various terms. This means that the effects of particle-particle interaction are ignored. The basic assumption for using the Euler–Lagrangian model is its lower volumetric percentage. Therefore, the presence of particles in the continuous phase has been shown to be effective. The governing equations for the incompressible laminar flow of the continuous phase are as follows:

$$\nabla \cdot \left(\rho \vec{v}_f\right) = 0 \tag{1}$$

$$\nabla \cdot \left(\rho \vec{v}_f \vec{v}_f\right) = -\nabla p + \nabla \cdot \left(\mu \nabla \vec{v}_f\right) + \vec{S} \tag{2}$$

where ρ is the fluid density, p is the fluid pressure, and $\vec{v}_f$ is the velocity vector for fluid flow. $\vec{S}$ is the source term for the momentum equation and is due to the presence of particles in the continuous phase. When the particles pass through the control volume or the computational mesh consisted of elements with a given volume δv, water fluid could be obtained from the formula below [13]:

$$\vec{S} = \sum_{i=1}^{\mathrm{np}} \frac{m_i}{\delta v} \vec{a} \tag{3}$$

where np is the number of particles in the volume control cell δv. The position of the particles is calculated as:

$$\hat{k} z_p(t) + \hat{j} y_p(t) + \hat{i} x_p(t) = \vec{r}_p \tag{4}$$

According to Newton's second law, the particle motion can be expressed as:

$$\vec{v}_p = \frac{d\vec{r}_p\left(x,y,z,t\right)}{dt} = \frac{dx_p}{dt}\hat{i} + \frac{dy_p}{dt}\hat{j} + \frac{dz_p}{dt}\hat{k} \tag{5}$$

$$\frac{d\vec{v}_p}{dt} = \vec{a} = \vec{a}_D + \vec{a}_B + \vec{a}_M + \vec{a}_E + \vec{a}_{\mathrm{Ma}} + \vec{a}_g \tag{6}$$

Here, $\vec{a}_D, \vec{a}_B, \vec{a}_M, \vec{a}_E, \vec{a}_{\mathrm{Ma}}, \vec{a}_g$ are the forces of unit mass or acceleration that denote the drag forces, Brownian force, magnetic force, electric force, Magnus force, and gravity, respectively. Most of these forces influence large particles and can be discarded for particles in the nanoscale size.

The drag force can affect the particle due to the relative velocity of the particle and the fluid. Particularly for Reynolds number < 100, the drag force is the dominant force that causes the particle to move [14]. The acceleration of drag force is obtained by the following equation [15]:

$$\vec{a}_D = \frac{18\mu_f C_D \mathrm{Re}_p}{24\rho_p d_p^2}\left(\vec{v}_f - \vec{v}_p\right) = \frac{1}{\tau_p}\left(\vec{v}_f - \vec{v}_p\right) \tag{7}$$

Here, Re_p is the Reynolds number of the particle, $\vec{v}_f, \vec{v}_p$ are the velocity of, respectively, the fluid and the particles, ρ_p is the density of the fluid, d_p is the diameter of the fluid, μ_f is the fluid viscosity, C_D is the drag coefficient, and τ_p is the particle relaxation time as defined below:

$$\mathrm{Re}_p = \frac{\rho_p d_p}{\mu_f}\left|\vec{v}_f - \vec{v}_p\right| \tag{8}$$

$$\tau_p = \frac{4}{16}\frac{\rho_p d_p^2}{\mu_f C_p \mathrm{Re}_p} \tag{9}$$

Due to the existence of the Brownian force, the acceleration comes from the random collision of particles with fluid molecules [16] in favor of submicron particles in the water. This force is quite significant for submicron particles because of the water molecules of less than 100 nm size [17]. The Brownian force is dominant for particles in the near-wall region where the viscous effects severely spread all over the fluid and flow speed moves slowly under reduced fluid velocity to zero. This force implies that the collision of particles occurs randomly and the fluid or gas consists of submerged atoms. The magnitude of the force is given by [14]:

$$a_{Bi} = \xi_i\sqrt{\frac{\pi S_0}{\Delta t}} \tag{10}$$

where ξ_i is the independent Gaussian random number, πS_0 is the unit variance, Δt is time variation. The components of the Brownian force are modeled as a Gaussian white noise process with spectral intensity given by [18]:

$$S_{n,ij} = S_0\delta_{ij} \tag{11}$$

In the above equation, δ_{ij} is the Kronecker delta constant. If both variables were of equal value, the value of delta 1 would otherwise be zero. S_0 is defined as follows:

$$S_0 = \frac{216\nu k_B T}{\pi^2\rho d_p^5\left(\frac{\rho_p}{\rho_f}\right)^2 C_c} \tag{12}$$

In Eq. (12), T is the absolute temperature of the liquid, ν is the kinematic viscosity, and C_c is the Stokes–Cunningham slip correction obtained from Eq. (13). In this formula, Boltzmann's k_B is set equal to 1.38×10^{-23}.

Taking account, the Boltzmann's $k_B = 1.38 \times 10^{-23}$ yields.

$$C_c = 1 + \frac{2\lambda}{d_{ij}}\left(1.257 + 0.4e^{-\frac{1.1d}{2\lambda}}\right), \tag{13}$$

$$d_{ij} = \frac{1}{2}\left(u_{i,j} + u_{j,i}\right) \tag{14}$$

In the present case, the deformation-rate tensor d and λ is the free path of the liquid molecule [19].

Magnetism and permanent electromagnetism in microscopic dimensions tend to saturate electromagnetic particles with an increasing magnetic field (greater than 0.5 Tesla). In this situation, the particles act like a permanent magnet. Calculation of the magnetic field involves a lot of deal of resources and relationships depending on the field and particle size and other parameters. The following equation is used for the calculation of the magnetic force on the particle [20].

$$\vec{a}_B = q\vec{v} \times \frac{\vec{B}}{m_i} \tag{15}$$

where x is the cross product, q is the electric charge of a particle, $\vec{B}$ is the magnetic field, $\vec{v}$ is the particle velocity. Magnetic and electrical forces are applied in the z-direction and found to have an impact on particles. The electric force generated by the electric field can be obtained as follows:

$$\vec{a}_E = \frac{q\vec{E}}{m_i} \tag{16}$$

Here, $\vec{E}$ is the electric field, $\vec{a}_E$ is the electric force of the unit mass entering the particle. The gravitational acceleration force is also $\vec{a}_g = \vec{g}$. The Magnus lift force is obtained on the particles in the rotating flow. The lift is by the pressure differential along a particle's surface also has an acceleration calculated as follows:

$$\vec{a}_{\mathrm{Magnus}} = 0.5C_M\rho_f A_p r_p \frac{\left(\left(\vec{\omega}_f - \vec{\omega}_p\right)\times\left(\vec{v}_f - \vec{v}_p\right)\right)}{m_i} \tag{17}$$

Here C_M is the constant of the force, ρ_f is the fluid density, A_p is the particle cross-section, ω is the particle angular

velocity with mass m_i, and $\vec{v}$ and $\vec{\omega}$ are, respectively, the linear and angular velocity.

3. Numerical simulation

We used a personal code for simulation. But given that this code is on developing. We are notable to publish the code. The results have been obtained by using open source SimFlow 3.1 post-processor software (free version_ https://sim-flow.com/download-simflow/).

3.1. Geometry, computational grid and physical properties of particles and fluid

Fig. 1 shows the schematic and geometric dimensions and the mode of separation of loaded particles. The separator consists of a seawater entrance and three outputs. The purified water is recovered from the middle of the outlet region. By the action of the electric field, ionization of the seawater occurs and attracts the positive and negative salt ions. In addition to the transmission of ions as the result of the electric field, a magnetic field is required for the enhancement of ions conduction to the upper and lower outlets. Fig. 1 illustrates the forces acting on charged particles. The particles rise to the upper and lower outlets by a sufficient amount of the forces to fully serve the separation process. Under these conditions, the intensity of the electric and magnetic fields, the particle diameter, the water velocity, and the flow regime are of great importance. As the Alnaimat et al. [9], the dimensions of the separator are considered with a cross-section of 20 cm × 10 cm and a length of 60 cm.

The thermophysical properties of seawater are evaluated by the separator. Table 1 shows the properties of the materials used in this study. The inlet temperature is found to be 297 K for seawater.

3.2. Independence of the results on the number of grids

Ensuring an independence number of grid model, mesh independence of the solution was checked in this section. As can be seen from Table 2, increasing type 3 number of cells did not significantly change the maximum fluid outlet speed. No change was observed in the third digit of the velocity after using a mesh of 3.8 million elements. This case implies that the mesh independence of the model was achieved. Raising the mesh to 4.5 million elements, the maximum speed in the output did not raise. Modeling grid type 3 was used to reduce the time and cost of modeling. The system specifications and the estimated Central Processing Unit time for modeling are shown in Table 2.

Fig. 2 shows an overview of the grid. According to the figure, the structure comprises meshes in the form of a regular hexagonal grid. The meshes element size is around 1 mm.

4. Results

Here, we will see that the results of this study indicate the efficiency of this system in the separation of particles (desalinating). As mentioned, due to the simultaneous application of the electric field and magnetic field, we expect the particle to be well absorbed. This section explores the findings of this research.

4.1. Flow velocity effect on the separation rate

Fig. 3 shows the percentage of adsorbed particles with different inlet flow rates. Desalination was modeled on the basis of studies by Alnaimat et al. [9]. The experiment parameters were including particle diameter 1 μm, the intensity of the magnetic field 0.2 Tesla and the electric field voltage 1 V. According to Fig. 3, with increasing fluid velocity from 0.1 to 0.5 m/s, the rate of separation felt decreases of 30%. In order to ensure the accuracy of the results, the findings of Alnaimat et al. [9] are also presented here.

Fig. 3 reveals the separation rate with different inlet flow rates. According to this figure, the percentage of separation decreased with increasing fluid velocity. As a result, a greater increase in the velocity of the fluid resulted in an additional reduction of the separation rate at the

Table 1
Pure water and salt particles properties

	Salt	Pure water	Unit
Density	2,160	998.2	(kg/m^3)
Viscosity	Not applied	0.00103	kg/(m s)
Magnetic permeability	1.35 e-6	1.275 e-6	h/m
Diameter	10^{-4} ~ 10^2 [16]	Not applied	μm
Temperature	297	297	°C

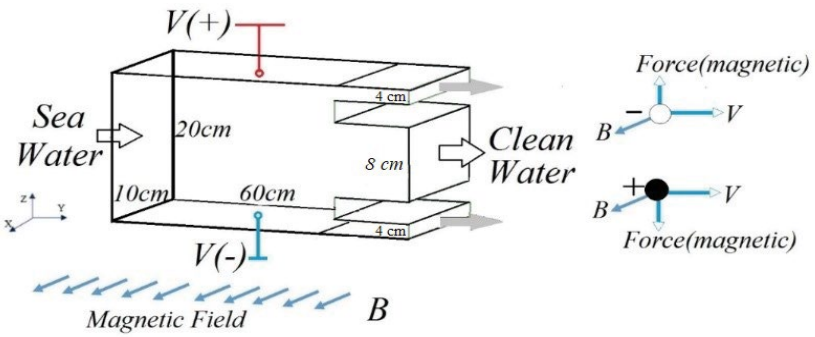

Fig. 1. Schematic of separator, dimensions, and boundary conditions.

Table 2
Mesh independency study and used system specifications

Mesh type	1	2	3	4
Total number of cells	3,000,000	3,800,000	4,500,000	7,000,000
Central Processing Unit time	1 h and 50 min	2 h and 25 min	4 h and 43 min	8 h and 17 min
Maximum water velocity at the outlet (m/s)	3.810	3.915	3.931	3.931
Processor	Intel(R) Core (TM) i7-6500U@3.1 GHz			
Random-Access Memory	16.0 GB			

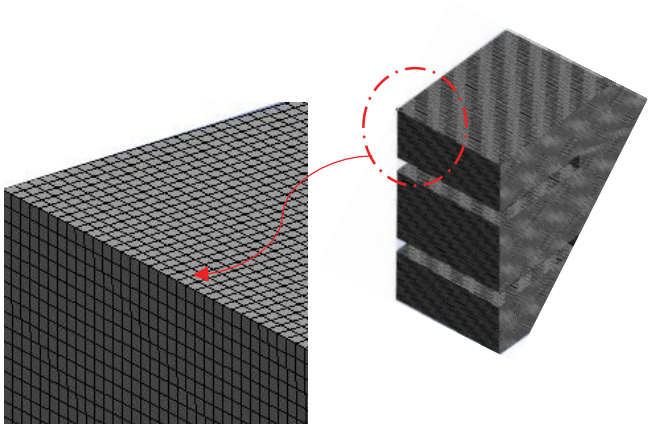

Fig. 2. Hexahedral mesh and element size.

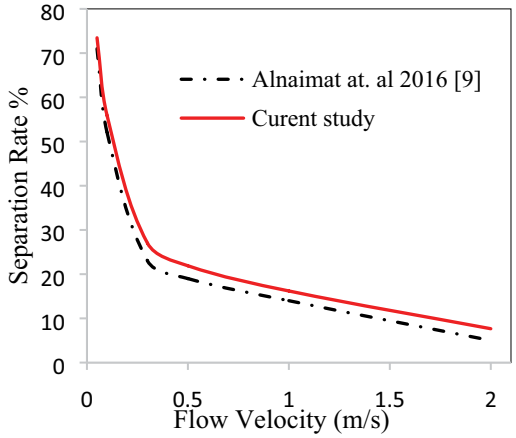

Fig. 3. Effect of change in fluid inlet velocity on particle separation rate.

lower slope. Eventually, at a fluid velocity of 2 m/s, the separation rate reached 6.6%, which represents the low efficiency of the device at this speed. Comparing these results with the findings Alnaimat et al. [9] obtained shows the similarity of the values and behavior of the obtained graphs. The difference between the results of the present work and that of Alnaimat et al. [9], might be due to modeling differences and hypotheses. It should be noted that the gravity force was not simulated in the two-dimensional symmetric model of Alnaimat et al. [9] study. Nonetheless, our simulation consists of a three-dimensional structure under the influence of the Brownian intermolecular forces and gravity.

4.2. Effect of electric and magnetic fields on particle absorption

As was already mentioned, using simultaneous electric and magnetic fields has been an effective method for separating particles from saline water. Our results, therefore, can be applied to improve the efficiency of desalinating water. To verify the modeling results in this study, the previous modeling was used. The velocity of the fluid and the particles in the entry are equal to 0.1 m/s. Clearly, the separation of particles in the discharge and greater fluid velocities require a bigger device. It needs to be emphasized that the particle diameter of this study and those of seawater were of the same size in terms of nanoscale and microscope [12]. Particles randomly entered the channel for the approximation to reality and increased the accuracy of results. Considering the fact that electric and magnetic fields are varying in intensity, the effect different intensities of the electric and magnetic fields on the separation were analyzed. As shown in Fig. 4, the particle movement was, initially, studied in the absence of electromechanical fields.

Figs. 4a and b show the fluid velocity and the speed of particle distribution applied to the channel in the absence of electric and magnetic fields. According to these figures, the particles were controlled by fluid flow and were mixed with the fluid once they entered the channel. The particles and fluid were catapulted at 0.1 m/s into the channel and passed through the output at approximately 0.2 m/s. The separator near the end of the channel could be the reason for increasing both particles and fluid at the outlet and cause a fluid axial acceleration by decreasing the cross-section. In the following, the effect of using both electric and magnetic fields on the separation process is investigated by applying different amounts of forces to the system. The particle concentration in the outputs is then reviewed.

Fig. 5 illustrates four cases for outlet particle concentration with different values of magnetic field (a) 0.2 Tesla, (b) 0.02 Tesla, (c) 0.07 Tesla, and (d) 0.007 Tesla. In each magnetic field, the voltage has three values of 0.2, 1, and 2 V. As shown in Fig. 4a, at the voltage of 2 V and the magnetic field of 0.2 Tesla, the maximum separation is obtained. In Fig. 4d, when a small magnetic field was applied, the efficiency of particle separation was not effectively increased, even by changing the electric field and increasing the voltage. Thus, the lowest degree of separation obtained at a voltage of 0.2 V and a magnetic field of 0.007 Tesla. The results

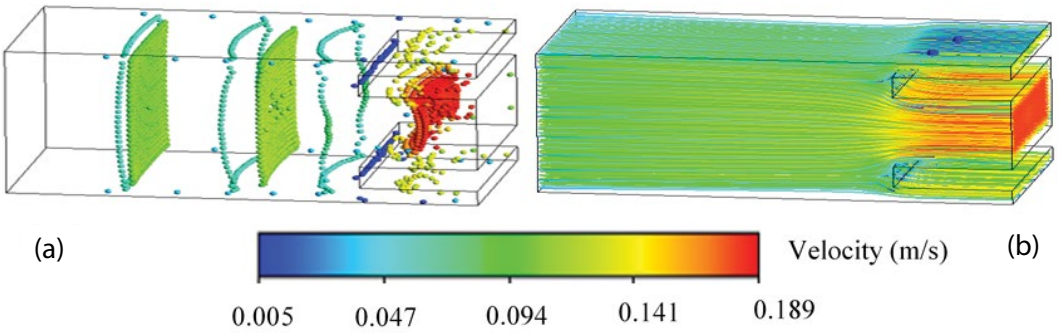

Fig. 4. (a) Distribution of particles and (b) flow lines in the separator system in the absence of electric and magnetic fields.

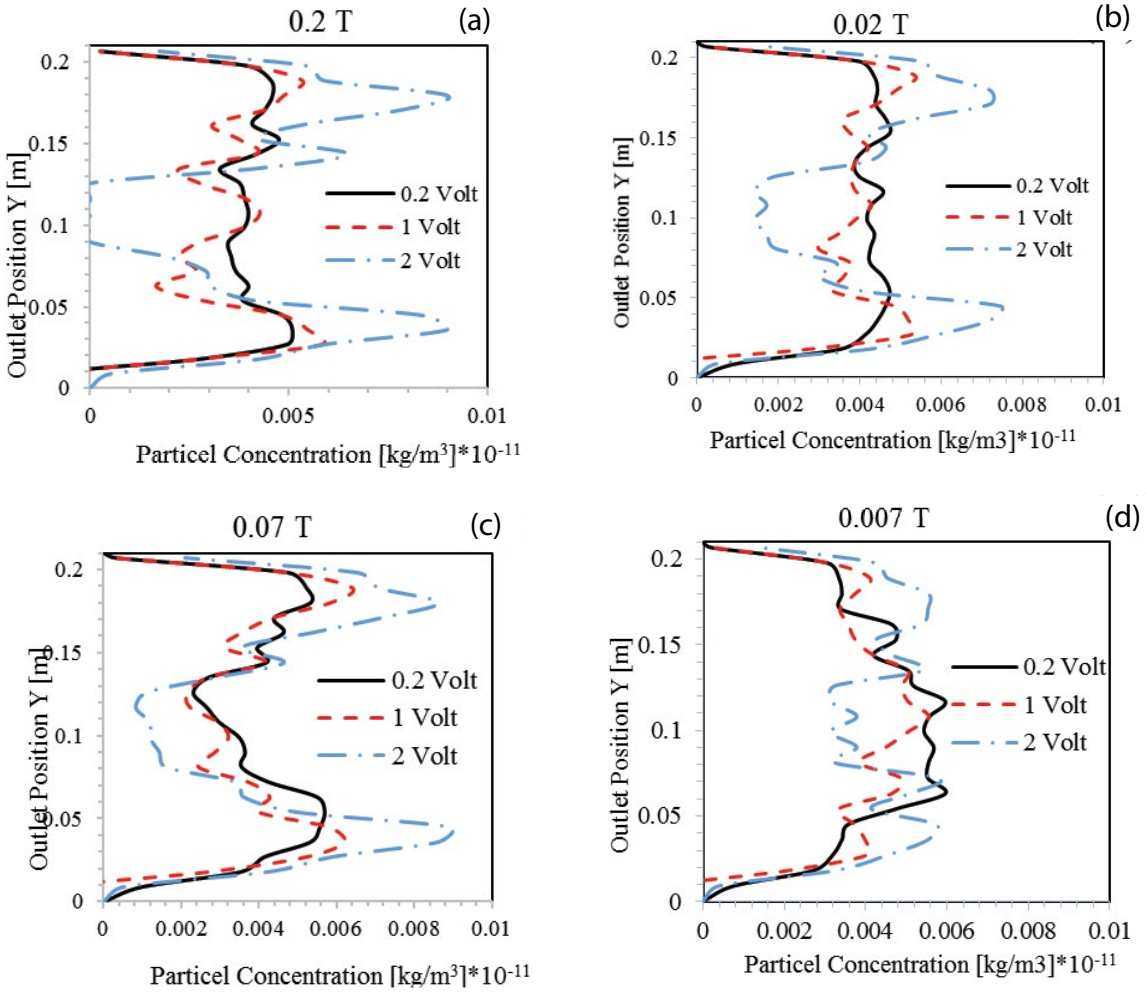

Fig. 5. Particle concentration at the outlet (a) B = 0.2 T, (b) B = 0.02 T, (c) B = 0.07 T, and (d) B = 0.007 T.

indicate that the magnetic field possesses a dominant role in particle separation.

4.3. Particles path by applying electric and magnetic fields

The particle motion pathway can be used to gain a better understanding of the behavior of the forces of the electric and magnetic fields. In Table 3, the position of a particle along the channel is reviewed. To understand the behavior of the particle along the channel, a closer examination is presented in Fig. 6. The position of the released particle from ($x0$, $y0$, $z0$) = (10, 10, 0).

The path of the motion of a particle with a diameter of 1 μm in an electric-magnetic field with a 1 V electric field and magnetic field intensity of 0.2 Tesla is depicted in Fig. 6. According to the figure, with the arrival of

Table 3
Sample particle path $P0 = (10,0,10)$

Z (cm)	10	10	9	8	7	7	8	10	10	10	13	15	17	18	19	20
Y (cm)	0	2	4	6	8	10	12	16	20	24	28	32	36	40	44	48
X (cm)	9.7	8	7.5	7.3	6.8	6.3	4.6	4.8	7.3	8.9	8.5	8.1	6.2	3.1	0.6	2.1

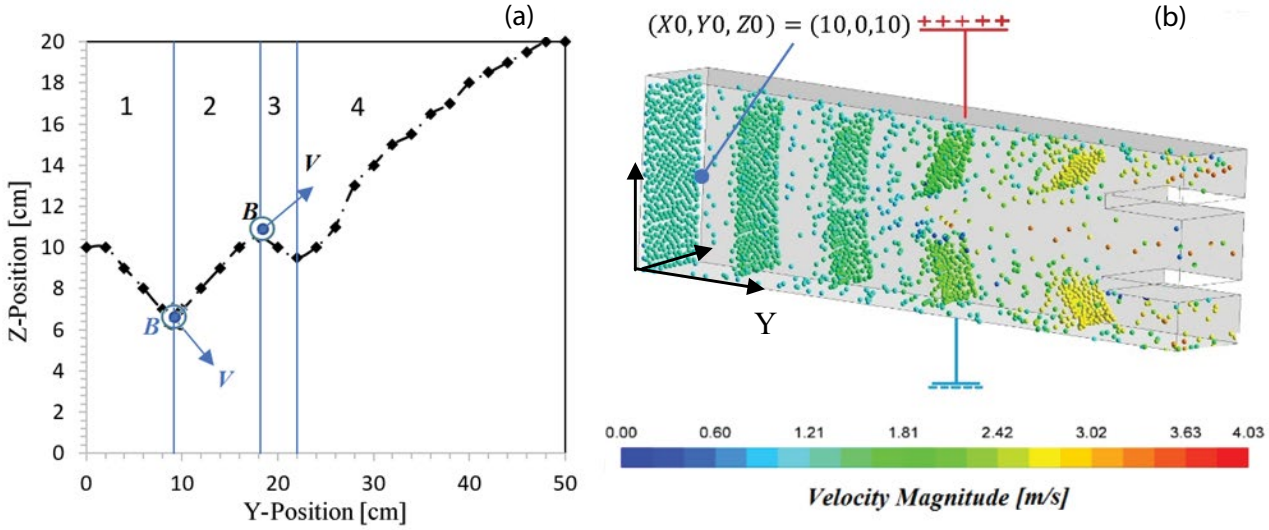

Fig. 6. (a) Path of a particle released at (10,0,10) and (b) velocity of particles, with a diameter of d_p = 1,000 nm along absorber channel under 1 V and magnetic field of 0.2 Tesla.

negative particles to the particle separator region, they become influenced by the weight force due to the particle density. Therefore, a migration of the particle flowing down an incline was observed. In the presence of weight, the forces generated by the electric field and the magnetic field have led to the indicated direction at the end of region 1 (Fig. 6a). Typically, these forces depend on the velocity and direction of the particle. Changes in the directions for regions 2 and 3 were also made. As the particle velocity was reduced by the drag force, the magnitude of the magnetic force to the upper wall was also reduced. This was due to the fact that the weight of particle became dominant which subsequently caused turning down of the particle into zone 3 of the particle path. Ultimately, the particle was moved toward the upper wall by controlling the magnetic and electrical forces.

4.4. Separation of seawater salt with different particle diameters

Two parameters including the fluid intake flow of 1 kg/s and the particle flow rate of 0.1 kg/s equal 10% of the mass of the fluid inlet were considered in this study. The separator system at a magnetic field of 0.2 Tesla and 0.02 Tesla with different voltages has been studied. The particle separation rate graph with different particle diameter and at different system voltage is shown in Fig. 7. In the magnetic field intensity of B = 0.2(T), the particles with a diameter greater than 50 μm to slightly higher than 57.77 μm become separated.

According to Figs. 7a and b, with increasing voltage, the particle separation rate was increased in both magnetic fields. After applying 1 V of the electric field, the separation of all particles continued at a very slight slope. With increasing the voltage in the magnetic field of 0.02 Tesla, the particle separation only continued for the particles larger than 1 μm. In the magnetic field of B = 0.2 Tesla, higher separation efficiency was observed. However, in the intensity of the strong magnetic field (B = 0.2 Tesla), the effect of increasing the voltages of more than 1 V on the separation was low. In other words, the application of a higher electrical field did not yield significant efficiencies in particle separation. Thus, when the magnetic field of 0.2 Tesla was used, the particle separation system did not operate well at voltages greater than 1 V. It should be noted that these results were collected by the current fluid flow conditions and by the system used in this research. Also, the results showed that by reducing the particle diameter from 1 μm to 1 nm, the efficiency of the separator system decreased. This could be due to the reduced effect of the electric-magnetic field on the particles. It seemed that the effect of the molecular electric field was higher on very small particles. However, the electric field effect on these particles in both magnetic fields was not significantly important. A comparison of Figs. 7a and b show that the change with the electric field was more effective in the separation of nano-sized particles. When the magnetic was weak, the separator required a higher voltage for particle separation. The reason for this is that with increasing to a magnetic field to

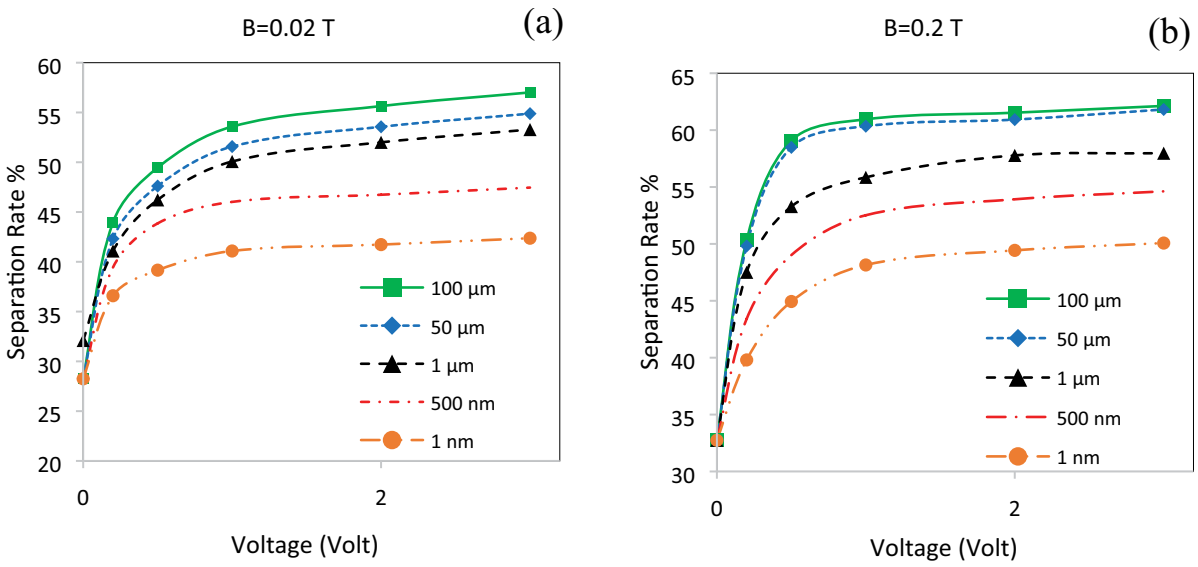

Fig. 7. Separation percentage of particles for d_p = 1 nm, 500 nm, 1 µm, 50 µm, 100 µm in different voltage for (a) B = 0.02 T and (b) B = 0.2 T.

ten-fold, the efficiency of separating particles at 1 V increases sharply to its maximum amount. In magnets of one-tenth, the maximum separation does not occur at a voltage of 3.

4.5. Brownian motion

With reducing the particle diameter to nanoscale size, a new particle behavior was observed in the separator system. Nanoparticles were affected by another type of intrinsic motion and molecular effects (i.e. irregular motion). The inertial force on nanoscale particles reduced the particle separation efficiency by overcoming the external electric force. Fig. 8 shows the effect of Brownian force on the particle separation.

As can be seen from Fig. 8a, particle separation efficiency felt a reduction and the maximum separation decreased from 50% to 48% in the strong magnetic field B = 0.2 Tesla. However, as shown in Figs. 8a and b, the presence of Brownian motion in low voltage (i.e. V = 0) did not affect the separation. This means that by increasing the voltage, the efficiency of the separation is increased from 32% to 48%, and the effect of the Brownian force is only about two to three percent at the highest voltage. Particle diffusion coefficients were compared with the diffusion coefficient of the

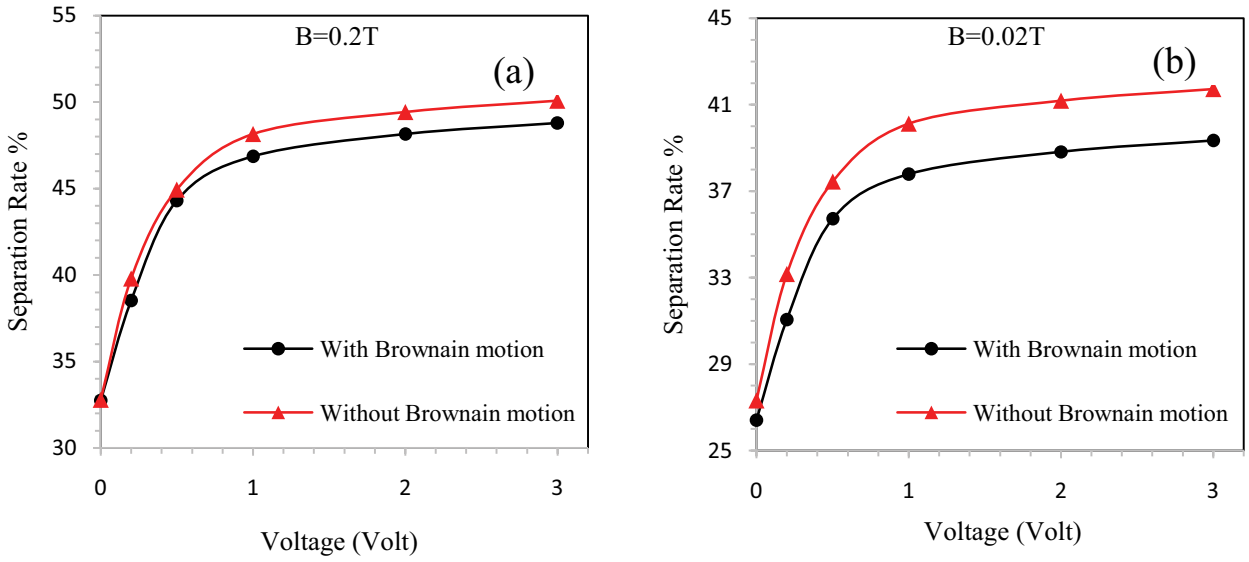

Fig. 8. Effect of Brownian force on the separation of particles with a diameter of d_p = 1 nm in a separator system under different electric field conditions and a magnetic field of (a) B = 0.2 and (b) B = 0.02 Tesla.

perforated force, and these penetration coefficients were determined in accordance with Eqs. (18) and (19).

$$D_B = \frac{KT}{3\pi\mu_f d_p} \tag{18}$$

$$D_T = \frac{\mu_f}{\rho_f T}\frac{\alpha_f}{2\alpha_f + \alpha_p} \tag{19}$$

where D_B is the diffusion coefficient, D_T is the thermal diffusion coefficient, K is the Boltzmann constant which is equal to 1.38e–23 kg m^2 K^{-1} s^{-2}, T is the fluid temperature, μ_f is fluid viscosity, d_p is particle diameter, ρ_f is the fluid density, α_f is the thermal permeability of the fluid, and α_p is the thermal permeability of the particles. The ratio of Brownian force on the thermal diffusion can be calculated using Eqs. (18) and (19):

$$N_{BT} = \frac{\left(D_B / \nabla T\right)}{D_T} \tag{20}$$

It should be noted that the Brownian force was effective on the nanosized particles. Table 4 shows the effect of the Brownian diffusion ratio on thermal diffusion for different particle diameters. According to Table 4, the separation efficiency was reduced by 6.4% for particles with a diameter of 10 nm. For particles larger than 5 nm, it seemed that the effect of the Brownian force was reduced. Thus, the separated particles under the influence or absence of this force were separated by a closer approximation.

As can be seen in Table 4, by reducing the particle diameter to 0.1 nm, the separation rate was reduced to approximately 37%. According to the above results, it can be said that the system needs to be recirculated in the system several times for particles smaller than 0.1 nm.

Fig. 9 shows the separation of nanoparticles with diameters less than 5 nm in the presence of the Brownian force. As already mentioned, the particle separation decreased with the application of the Brownian motion. According to Fig. 9, it may be necessary to circulate fluid several times at 1 V or higher for the separation of particles smaller than one nanometer. By reducing the particle diameter to 0.1 nm, the effect of the system on the separation appreciably reduced, which is a diameter of 5 nm had a maximum separation rate of 47%. While this value decreased by approximately 33% for the particle diameter of 0.1 nm.

Fig. 10 shows the path of the particle movement, as well as the particle concentration in the magnetic field of 0.2 Tesla, and the potential of the voltage of 1 for the particle diameter of 5 nm. As can be seen, the system failed to separate a large part of the particles, and some particles were not affected by electric and magnetic influences. By calculating this contour, we can calculate the separation percent.

4.6. Effect of the separation system inlet aspect ratio on the percentage of separation

The geometry of the separator system was effective in the rate of desalination. Therefore, the geometry changes were analyzed in this section. First, the separator system was reviewed in three different aspect ratios which are presented in Table 5.

As shown in Table 5, the geometries examined are of a kind that, in all models, the overall volume is the same.

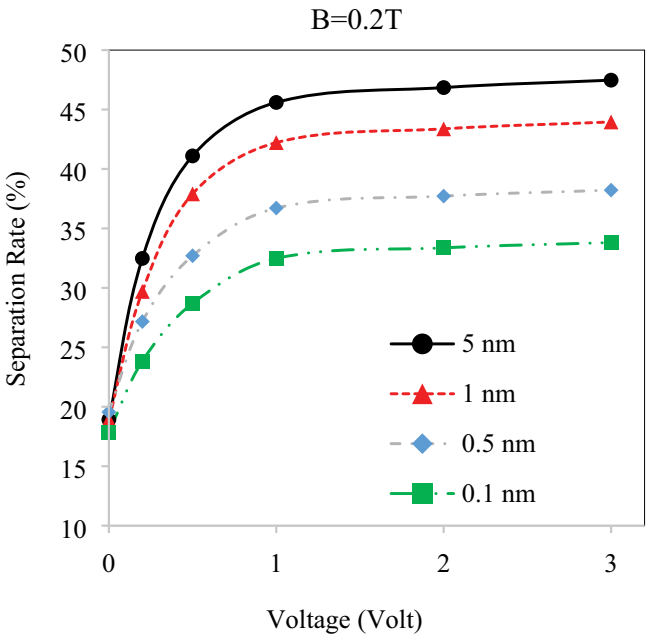

Fig. 9. Characterization of nanoparticles with different diameters along the adsorbent channel under various electric fields and magnetic fields 0.2 Tesla.

Table 4
Brownian permeability diffusion ratio to thermal permeability in particles with different diameters

d_p (nm)	N_{BT}	Separation rate		Difference %
		With Brownian	Without Brownian	
5	4.71	52.77%	54.24%	1.47%
1	6.1	48.78%	50.07%	1.29%
0.5	9.97	42.42%	46.74%	4.32%
0.1	15.42	37.52%	44.41%	6.89%

Table 5
Geometry in a different aspect ratio

Inlet aspect ratio (a/b)	Inlet cross section ($a \times b$)	V (m^3)	System length (m)
0.5	0.1 × 0.2	0.012	0.6
1	0.142 × 0.142	~0.012	0.6
1.5	0.2 × 0.1	0.012	0.6

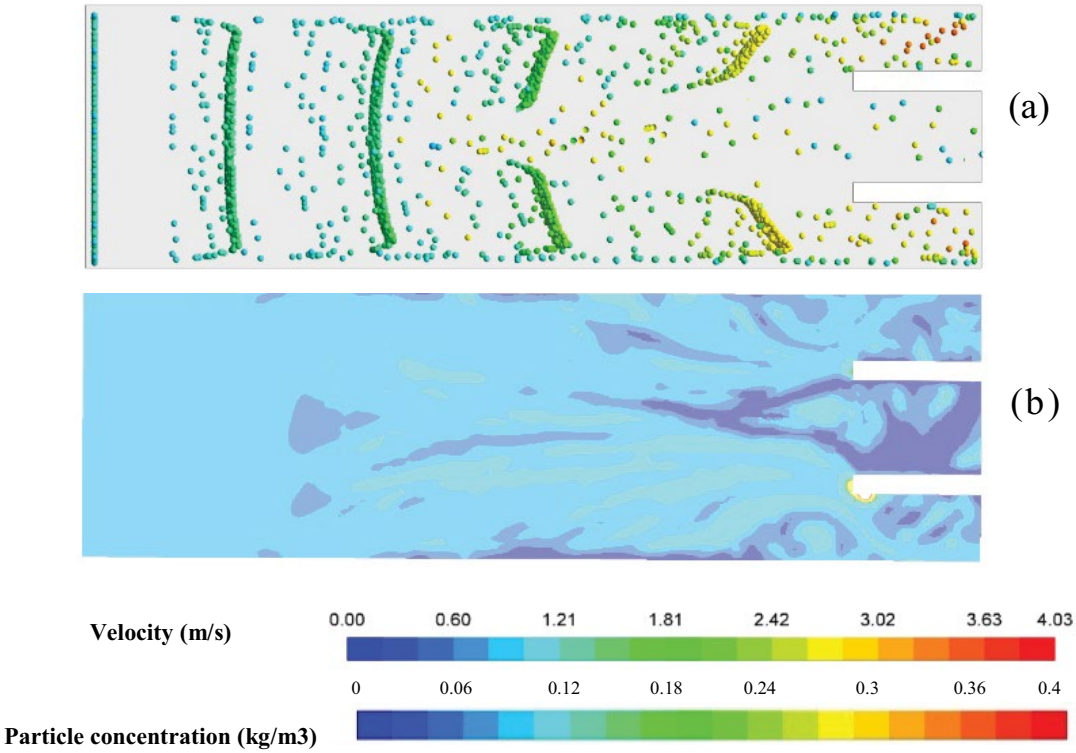

Fig. 10. (a) Particle velocity v_p and (b) particle concentration contour.

The effect of geometry changes on the degree of separation is examined by magnetic-electric forces with B = 0.2 Tesla, V = 1 V, and particle diameter of d_p = 1 μm. In Fig. 11, the proposed changes in the aspect ratio on the degree of separation is depicted. This figure shows that the least degree of separation occurred in A.R. = 0.5. According to the studies, by decreasing the ratio of the dimensions, the distance between the polar field of the electric field is diverted. Hence, the impact of separation systems on particles in the center of the system was decreased. By changing the aspect ratio to the value of 1, the impact of electrical and magnetic on the system can be maximized. This caused all particles to be placed in both electric and magnetic fields. The performed studies indicate that by changing the geometry of the isolation system to a ratio of 1, the highest separation efficiency can be created. Also, a change in the length of the core system can be an effective way of increasing the amount of separation. Increasing the length of the separator system increased the duration of the particles in the electrical and magnetic flows. Fig. 12 shows the amount of separation of particles at different intervals of the system.

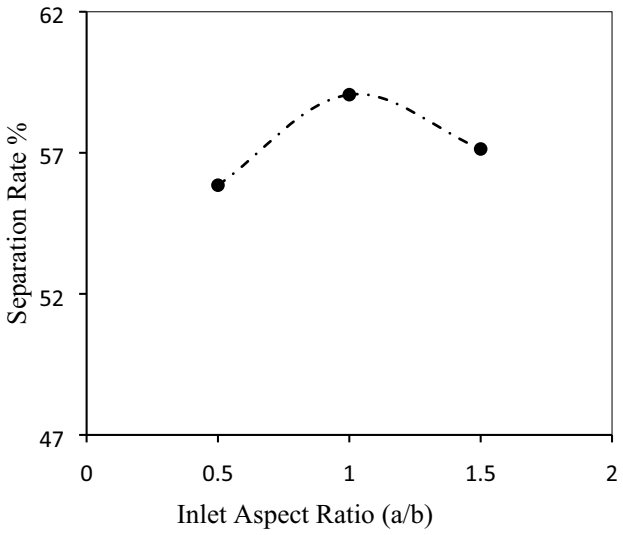

Fig. 11. Particle absorption percentage for different inlet cross section aspect ratios, d_p = 1 μm, $v_f = v_p$ = 0.2 m/s, B = 0.2 T, V = 1 V.

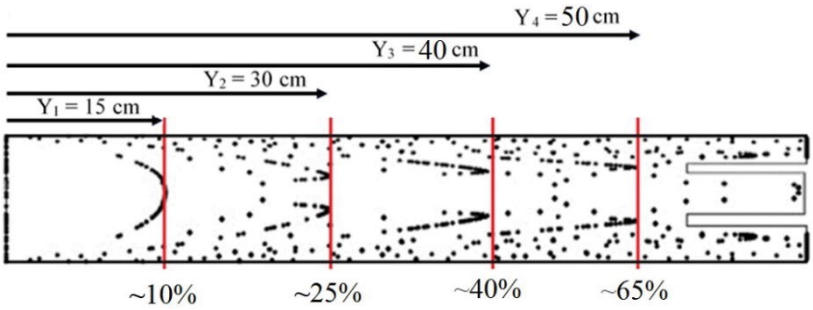

Fig. 12. Effect of increasing the length of the channel on the percent of particle separation.

As shown in Fig. 12, with an increase in the length of the separation system, the amount of sweetening water increased from 10% to about 65%. However, it is seen, the separation value has not changed significantly after a distance of 50 cm. This can be attributed to the lack of adequate system impact on the particles in the channel center. Therefore, mixing the outlet water from the sweetener and using a water-ring can be re-introduced into the sweetening system to increase the percentage of particle separation.

5. Conclusion

Reducing the flow of fluid into the system can increase the system isolation power. But this increases the amount of time needed to desalinate a certain amount of water. Studies indicate that with increasing the fluid flow rate up to 0.1 m/s, recovery of purified water can be achieved. With the application of excessive voltage to the system, no significant effect was observed on increasing the amount of separation. Ibn Al-Am also boosts energy consumption and also increases system costs. Therefore, the most economical way to isolate the system studied in this study is to apply an electric current of 1 V and a magnetic field 0.2 Tesla. The physical structure of the separation system can be an effective way of increasing the amount of separation. As previously mentioned, these changes can increase the amount of desalinated water by about 4%. Also, increasing the length of the isolation system to a certain amount increased the amount of desalinated water. Reducing the particle diameter to the nanoparticle range has increased the power of the brawn. This results in unwanted motion in the particles and a decrease in the strength of the particles from the electrical and magnetic flux. Using a separator system, up to 60% can perform the desalination process. However, increasing the yield requires successive loops to increase separation percentages.

Data availability

All data generated or analyzed during this study are included in this article.

Author contributions

All modelling and analyzed the results jointly conducted by M.V.N and H.R.N. All the authors analyzed and discussed the achieved results, and reviewed the manuscript.

References

[1] P.K. Goel, Water Pollution: Causes, Effects and Control, New Age International, 2006.
[2] S.A. Morsi, A.J. Alexander, An investigation of particle trajectories in two-phase flow systems, J. Fluid Mech., 55 (1972) 193–208.
[3] T. Mohammadi, A. Kaviani, Water shortage and seawater desalination by electrodialysis, Desalination, 158 (2003) 267–270.
[4] V.C. Loukopoulos, E.E. Tzirtzilakis, Biomagnetic channel flow in spatially varying magnetic field, Int. J. Eng. Sci., 42 (2004) 571–590.
[5] T. Mohammadi, A. Moheb, M. Sadrzadeh, A. Razmi, Separation of copper ions by electrodialysis using Taguchi experimental design, Desalination, 169 (2004) 21–31.
[6] U. Lehmann, S. Hadjidj, V.K. Parashar, C. Vandevyver, A. Rida, M.A.M. Gijs, Two-dimensional magnetic manipulation of microdroplets on a chip as a platform for bioanalytical applications, Sens. Actuators, B, 117 (2006) 457–463.
[7] E.P. Furlani, Y. Sahoo, K.C. Ng, J.C. Wortman, T.E. Monk, A model for predicting magnetic particle capture in a microfluidic bioseparator, Biomed. Microdevices, 9 (2007) 451–463.
[8] T.O. Nichols, System and Process for Extracting and Collecting Substances from a Molecular Combination, U.S. Patent No. 8,110,175, 7 February 2012.
[9] F. Alnaimat, E. Alhseinat, F. Banat, V. Mittal, Electromagnetic–mechanical desalination: mathematical modeling, Desalination, 380 (2016) 75–84.
[10] D. Zarzo, D. Prats, Desalination and energy consumption. What can we expect in the near future?, Desalination, 427 (2018) 1–9.
[11] A. Rozanska, J. Wisniewski, T. Winnicki, Donnan dialysis with anion-exchange membranes in a water desalination system, Desalination, 198 (2006) 236–246.
[12] T.R. Parsons, Y. Maita, C.M. Lalli, A Manual of Chemical & Biological Methods for Seawater Analysis, Elsevier, 2013.
[13] C.T. Crowe, T.R. Troutt, J.N. Chung, Numerical models for two-phase turbulent flows, Annu. Rev. Fluid Mech., 28 (1996) 11–43.
[14] Y. Tsuji, T. Kawaguchi, T. Tanaka, Discrete particle simulation of two-dimensional fluidized bed, Powder Technol., 77 (1993) 79–87.
[15] J.W. Haverkort, S. Kenjereš, C.R. Kleijn, Computational simulations of magnetic particle capture in arterial flows, Ann. Biomed. Eng., 37 (2009) 2436.
[16] T.F. Kong, H. Shin E, H.S. Sugiarto, H.F. Liew, X.H. Wang, W.S. Lew, N.-T. Nguyen, Y. Chen, An efficient microfluidic sorter: implementation of double meandering micro striplines for magnetic particles switching, Microfluid. Nanofluid., 10 (2011) 1069–1078.
[17] P. Xu, M. Capito, T.Y. Cath, Selective removal of arsenic and monovalent ions from brackish water reverse osmosis concentrate, J. Hazard. Mater., 260 (2013) 885–891.
[18] D.S. Wen, L. Zhang, Y.R. He, Flow and migration of nanoparticle in a single channel, Heat Mass Transfer, 45 (2009) 1061–1067.
[19] A. Li, G. Ahmadi, Dispersion and deposition of spherical particles from point sources in a turbulent channel flow, Aerosol Sci. Technol., 16 (1992) 209–226.
[20] R.D. Noble, S.A. Stern, Eds., Membrane Separations Technology: Principles and Applications, Vol. 2, Elsevier, 1995.